International Journal of Latest Research in Science and Technology **ISSN (Online):2278-5299**
Volume 2, Issue 5: Page No.18 -25 ,September-October 2013
https://www.mnkpublication.com/journal/ijlrst/index.php

NUMERICAL, TWO-DIMENSIONAL ABLATION MODEL FOR INTERFERING, HIGH POWER LASER BEAMS

Jan Marczak, Karol Jach, Robert Świerczyński, Marek Strzelec
Military University of Technology, Institute of Optoelectronics, Warsaw, Poland

Abstract*- The article presents two dimensional – 2D(x,y) numerical ablation model, which describes simultaneous interaction, in close proximity, of two and three high power pulsed laser beams. Such pulsed laser beams may be generated as a result of, e.g., interference of two high power pulsed laser beams. Geometry of the sample and method of its illumination were presented. Illuminated disk was constituted by an aluminium layer with a thickness of 400 nm, lying on a quartz substrate with a thickness of 900 nm. Results of numerical calculations, presented in the article, were selected from many previously-performed numerical simulations for two and three simultaneously interacting pulsed laser beams, dependent on their intensity and their reciprocal distance, taking into account the material parameters of the selected target. Equations describing the problem of interaction between high power pulsed radiation and an aluminium target, which were presented and described in the article, were solved numerically using the free particle method.

Keywords - 2D(x,y) numerical model; pulsed laser; direct lithography; interference; laser ablation

INTRODUCTION

One of the important issues in the area of materials engineering is conscious surface modification of different materials, e.g. manufacturing of micron- and submicron structures. Surfaces of solids may be modified in various ways in order to meet physical, chemical, or mechanical requirements, such as, e.g., wear resistance, decrease in resistance to flow, change of tribological properties, change of light reflectance, or protection against corrosion [1]. Modified and innovative surfaces will be effective if they are arranged in a suitable place having relevant technical property and efficiency.

Some surface properties need structure dimensions in the range of several to dozens of micrometers (e.g., manufacturing of oil containers - lubrication of sockets in deep cavities or ink pots in printing dies, creating undulating surfaces of "shark skin" type or adapting the surface structure to different forms). Significantly smaller structures are needed for other surface properties (e.g. protection against wear by depositing hard phases in elastic matrix, "lotus flower" self-cleaning effects, local colour changes, change of adhesion and sealing effects). As a consequence, there is a need for several techniques of surface structuring aimed at creating a particular texture having different scales and properties.

In recent decades, many different techniques for shaping - structuring of surfaces in the micro-and nanometric scale have been developed. One of the recent ones is the Direct Laser Interference Lithography (DLIL) [1-3], using high power lasers emitting radiation in the range of UV, VIS and NIR, e.g. Q-modulated Nd:YAG laser. As a result of photothermal, photochemical or photophysical impact [4], surfaces of materials can be modified directly and locally in places corresponding to maximal interference. Since various metallurgical effects can also be induced (especially in metals and ceramics), this method is called the Laser Interference Metalurgy (LIMET) [5]. Formation of periodic 1D, 2D and 3D structures on the surface and in the volume of materials of micro-and submicron dimensions is a developing field of research with applications in many areas of technology [6, 7]. One example is a bone material presenting complex hierarchical structure of short-ranged, orderly distribution of fibers and particles and with long-ranged, orderly, periodic structure, on which there are several hierarchical levels with dimensions from nanometers to micrometers and even as large as millimeters [8]. This type of structure on the surface of metals, semiconductors, dielectrics or polymers allows to generate new properties of materials of very specific optical, electrical, mechanical, chemical and even biomedical characteristics [9].

Direct interference lithography is based on the spatial variations of radiation intensity generated as a result of interference of at least two pulsed laser beams, which can induce local and periodical modifications of the material surface. This allows, in one step and without the mask, for a direct production of periodic structures and patterns with well-defined long-ranged order in the micro- and submicron scale. This technique is a new solution for initiation of metallurgical processes, such as melting, recrystallisation, or regeneration of the surface layer of materials. The use of high-power pulsed lasers allows to modify the morphology and structure of the outer layer or layers (melting of deeper layers) or without melting of material lying below [10]. Depending on the specific material parameters and morphology of structures, new systems, such as bio-sensors [11], micro-flow systems [12], photonic structures [13] and mechanical parts with increased lifetime [14] can be realised.

Publication History
Manuscript Received : 22 October 2013
Manuscript Accepted : 27 October 2013
Revision Received : 28 October 2013
Manuscript Published : 31 October 2013

The article presents:

- Original, two-dimensional 2D(x,y) numerical model describing the issue of material ablation.
- Preliminary computer simulations for power density of radiation flux of the order of: $q \approx 10^8 \div 10^{10}$ $[W/cm^2]$.
- Results of numerical calculations for the problem of spatially periodic ablation of irradiated material, generated by periodic intensity distribution of the laser radiation produced, e.g., as a result of interference of two laser beams.
- Selected experimental example of the structure obtained has been given.

I. THEORY

A. Equations of the problem

A basic system of partial differential equations describing the analysed problem is based on the laws of conservation of mass, momentum and energy for elasto-plastic bodies. In the axially-symetrical case 2D(r,z) the model is the following [15-18] (cylindrical symmetry; planar symmetry equations obtained using asymptotic transition $r \to \infty$ and variable substitution $(r,z) \to (x,y)$):

$$\frac{d\rho}{dt} + \rho div\vec{w} = 0 \tag{1}$$

$$\rho\frac{du}{dt} = -\frac{\partial p}{\partial r} + \frac{\partial S_{rr}}{\partial r} + \frac{\partial S_{rz}}{\partial z} + \frac{S_{rr} - S_{\varphi\varphi}}{r}$$

$$\rho\frac{d\upsilon}{dt} = -\frac{\partial p}{\partial z} + \frac{\partial S_{rz}}{\partial r} + \frac{\partial S_{zz}}{\partial z} + \frac{S_{rz}}{r} \tag{3}$$

$$\rho\frac{de}{dt} = -pdiv\vec{w} + S_{rr}\frac{\partial u}{\partial r} + S_{\varphi\varphi}\frac{u}{r} + S_{zz}\frac{\partial \upsilon}{\partial z} + S_{rz}\left(\frac{\partial u}{\partial z} + \frac{\partial \upsilon}{\partial r}\right) \tag{4}$$

$$-\rho Q_m\frac{d\alpha_m}{dt} - \rho Q_e\frac{d\alpha_e}{dt} - \frac{\partial q}{\partial z} - Q_S + Q_T - Q_R$$

$$\frac{dS_{rr}}{dt} = 2\mu\left(\frac{\partial u}{\partial r} - \frac{1}{3}div\vec{w}\right) + \left(\frac{\partial u}{\partial z} - \frac{\partial \upsilon}{\partial r}\right)S_{rz} \tag{5}$$

$$\frac{dS_{\varphi\varphi}}{dt} = 2\mu\left(\frac{u}{r} - \frac{1}{3}div\vec{w}\right) \tag{6}$$

$$\frac{dS_{zz}}{dt} = 2\mu\left(\frac{\partial \upsilon}{\partial z} - \frac{1}{3}div\vec{w}\right) - \left(\frac{\partial u}{\partial z} - \frac{\partial \upsilon}{\partial r}\right)S_{rz} \tag{7}$$

$$\frac{dS_{rz}}{dt} = \mu\left(\frac{\partial u}{\partial z} + \frac{\partial \upsilon}{\partial r}\right) - \frac{1}{2}\left(\frac{\partial u}{\partial z} - \frac{\partial \upsilon}{\partial r}\right)\left(S_{rr} - S_{zz}\right) \tag{8}$$

where: ρ – density, p – pressure, e – internal energy per unit mass, u – mass velocity along r axis, υ – mass velocity along z axis, S_{ik} – stress tensor deviator components, μ – shear modulus, q – laser beam flux, Q_m – latent heat of melting, Q_e – latent heat of evaporation, α_m – coefficient of phase transition to liquid, α_e – coefficient of phase transition to gas, Q_S – ionisation losses, Q_T – an expression describing heat conduction, Q_R – radiation losses. The substantial derivative d/dt and the expressions $div\vec{w}$ are in the assumed coordinate system defined as follows:

$$\frac{d}{dt} = \frac{\partial}{\partial t} + u\frac{\partial}{\partial r} + \upsilon\frac{\partial}{\partial z};\ div\vec{w} = \frac{\partial u}{\partial r} + \frac{\partial \upsilon}{\partial z} + \frac{u}{r} \tag{9}$$

Derivatives $d\alpha_m/dt$ and $d\alpha_e/dt$ are expressed as follows:

$$\frac{d\alpha_m}{dt} = \frac{e - e_m}{Q_m\tau_m};\ 0 \le \alpha_m \le 1;\ e_m = c_V\left(T_m - 300\right) \tag{10}$$

$$\frac{d\alpha_e}{dt} = \frac{e - e_e}{Q_e\tau_e};\ 0 \le \alpha_e \le 1;\ e_e = c_V\left(T_e - 300\right) \tag{11}$$

where: e_m, e_e – internal energies corresponding to melting and boiling point, c_V – specific heat at constant volume, T_m – melting point, T_e – boiling point, α_m, α_e – relaxation times.

Let us move on to defining the expressions q, Q_T, Q_S i Q_R in the equation of energy conservation.

The laser radiation energy flux is expressed by the equation [19, 20]:

$$q = q_0(r,t)\exp\left[-\int_{z_0(r,t)}^{z} K dz\right], \tag{12}$$

with

$$K = K_0(\rho/\rho_0)^2(T_0/T)^{1/2}(Z/Z_0)^3\left[1 - \exp\left(-\frac{h\nu}{kT}\right)\right];\ (13)$$

and $\nu = \frac{c}{\lambda}$.

where: K – laser radiation absorption coefficient, q_0 – radiation energy flux on the deforming sample surface $z_0(r,t)$, T_0 – room temperature, ρ_0 – initial density, λ – laser wavelength, c – velocity of light, h – Planck's constant, k – Boltzmann's constant, Z – ionisation level, Z_0 – initial ionisation level, K_0 – constant coefficient.

Q_T is in turn an expression describing the phenomenon of classical heat conduction and χ is the coefficient of heat conduction:

$$Q_T = \frac{1}{r}\frac{\partial}{\partial r}\left(r\chi\frac{\partial T}{\partial r}\right) + \frac{\partial}{\partial z}\left(\chi\frac{\partial T}{\partial z}\right) \tag{14}$$

$$\chi = \chi_0\frac{T^{5/2}}{1+Z} + \chi_1 \tag{15}$$

where: χ_1, χ_0– constant coefficients.

Ionisation losses were introduced by defining the Q_S factor as follows:

$$Q_S = \rho\frac{J(Z)}{m_j}\frac{dZ}{dt} \tag{16}$$

where: $J(Z)$ – interpolated ionisation potential, m_j – mass of the nucleus. $J(Z)$ is determined by the formula:

$$J(Z) = J_0 + J_1\frac{Z^2}{(Z_j + 2/3 - Z)^{2/3}}, \tag{17}$$

whereby $J_0 = \dfrac{3}{1 - \dfrac{0{,}96}{(Z_j+1)^{0.257}}}$ [eV], J_1 = 11,26 [eV],

where: Z_j – nucleus charge.

The expression describing radiation losses Q_R is more complex due to the equation of conservation of radiant energy that has to be added to the computations [21]:

$$\rho\frac{de_r}{dt} = -p_r div\vec{w} + Q_R + \frac{1}{r}\frac{\partial}{\partial r}\left(rD\frac{\partial T_r}{\partial r}\right) + \frac{\partial}{\partial z}\left(D\frac{\partial T_r}{\partial z}\right), \tag{18}$$

$$Q_R = \rho K_{re}, \tag{19}$$

$$e_r = \frac{4\sigma T_r^4}{\rho c},\ p_r = \frac{4\sigma T_r^4}{3c} \tag{20}$$

where: e_r – radiant energy density; p_r – radiation pressure; T_r – radiation temperature, σ – Stefan-Boltzmann constant.

The diffusion coefficient D and the factor describing the exchange of radiant energy with the medium K_{re} is defined as follows:

$$D=\frac{16\sigma l_R T_r^3}{3};K_{re}=\frac{4K_p\sigma}{\rho}(T^4-T_r^4);$$
$$l_R=1{,}42\times10^{-8}\frac{AT}{(Z_j-Z)\rho};K_p=\frac{30{,}32}{l_R} \quad (21)$$

where: A – mass number, l_R – Rosseland range.

The relation between internal energy e with temperature T of the medium is defined as follows:

$$T=\frac{e}{c_V}+300 \quad (22)$$

where: c_V – specific heat at constant volume that with the impact of medium ionisation looks as follows:

$$c_V=c_{V0}\frac{(1+Z)}{(1+Z_0)} \quad (23)$$

The level of medium ionisation Z can be computed with the use of a collision-radiation model or the Saha equilibrium model [22]. In the collision-radiation model the level of ionisation is obtained by solving a differential equation in the form:

$$\frac{dZ}{dt}=Z(\nu_i-\nu_t-\nu_f) \quad (24)$$

where: ν_i – collision ionisation rate; ν_t – three-body recombination rate; ν_f – photo-recombination rate.

The analysed laser parameter range, meaning density and temperature of the irradiated medium, similar results can be obtained using the Saha equilibrium model. The computations are far simpler, as the ionisation level Z is determined using the following algebraic equation:

$$Z=\frac{3\times10^{23}}{n_j}\left[\frac{kT}{J_H}\right]^{3/2}\exp\left[-\frac{J(Z)}{kT}\right] \quad (25)$$

where: n_j – ion concentration; J_H – hydrogen ionisation potential (J_H = 13,6 [eV]).

Equations of state of the researched media have to be added to the system of equations above. The subject literature contains various forms of these relations: $p = p(\rho,e)$ or $p = p(\rho,T)$. In our research we use the following form of the equations of state [23, 24]:

$$p=p_x+\gamma\rho e \quad (26)$$

$$p_x=k_1(x^{\alpha_1}-x^{\alpha_2});x=\frac{\rho}{\rho_0} \quad (27)$$

where: p_x – is so called elastic pressure; k_1, α_1, α_2 – constants.

The system of equations (1) - (8) needs to be augmented by conditions determining the state when the medium changes from elastic to plastic properties. This condition was applied in the form proposed by Mises [15, 25]:

$$S_{rr}^2+S_{\varphi\varphi}^2+S_{zz}^2+2S_{rz}^2\le\frac{2}{3}Y^2 \quad (28)$$

where: Y – yield strength.

When this condition is exceeded, its fulfillment is guaranteed by so called stress scaling procedure for elastic-plastic behavior.

The yield strength Y and shear modulus μ were assumed as in the Johnson-Cook model [18]:

$$Y=\left[B+C(\varepsilon^p)^n\right]\left(1+E\ln\dot{\varepsilon}_*^p\right)\left[1-\left(T^*\right)^m\right] \quad (29)$$

$$\mu=\mu_0\left[1-\left(T^*\right)^m\right] \quad (30)$$

where:

$$T^*=\frac{T-300}{T_m-300};\varepsilon^p=\frac{\sqrt{2}}{3}\left[\begin{matrix}\left(\varepsilon_{rr}^p-\varepsilon_{zz}^p\right)^2+\left(\varepsilon_{rr}^p-\varepsilon_{\varphi\varphi}^p\right)^2\\+\left(\varepsilon_{zz}^p-\varepsilon_{\varphi\varphi}^p\right)^2+\frac{3}{2}\left(\varepsilon_{rz}^p\right)^2\end{matrix}\right]^{1/2};$$

$\dot{\varepsilon}_*^p=\frac{\dot{\varepsilon}^p}{\dot{\varepsilon}^0};\dot{\varepsilon}^0=1[1/\mathrm{s}]$, B, C, E, n, m – constants; μ_0 – constant; ε^p – equivalent plastic deformation; $\dot{\varepsilon}^p$ – plastic strain rate, ε_{ik}^p – plastic strain tensor components.

For $T > T_m$ the assumptions were $Y = 0$, $\mu = 0$ which is equivalent to transition to a hydrodynamic approximation.

B. Geometry of the model adopted for calculations

In laser interference lithography, picture of the full field $\vec{E}$ of many interfering laser beams is obtained as a result of superposition of each individual field $\vec{E}_j$ from each beam. This resultant field can be represented as follows:

$$\vec{E}=\sum_{j=1}^{n}\vec{E}_j=\sum_{j=1}^{n}\vec{E}_{j0}\cdot\exp\left[-i\left(\vec{k}\cdot\vec{r}-\omega\cdot t\right)\right] \quad (31)$$

where: $\vec{E}_{j0}$ - initial value of component beam electric field vector, $\vec{k}$ - wave number vector, $\vec{r}$ - radial coordinate vector, ω - angular frequency of electric field.

In this case, representation of the interference "2" of (two) laser beams is illustrated in Fig. 1. In maximal interference of the two beams, their intensities can be represented by the formula:

$$I=4I_0\cos^2(kx\sin\theta) \quad (32)$$

with the period of the fringe field:

$$d=\frac{\lambda}{2\sin\theta} \quad (33)$$

where: I - resultant intensity of laser beam in equation (32), I_0 - initial intensity of laser beam, θ - half-angle between interfering laser beams.

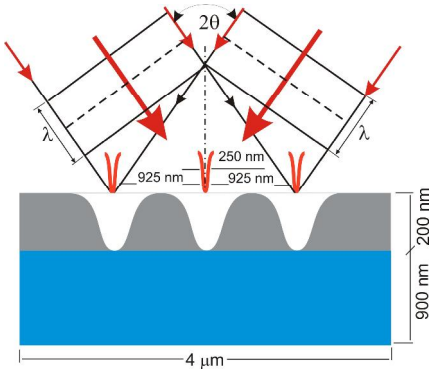

Fig.1. Illustration of interference of two plane waves. Angle between the beams is 2θ. Interference generates simple, equidistant interference fringes in the plane perpendicular to the drawing plane

Two overlapping laser beams, when falling on the surface of the material, produce periodic, linear picture of interference fringes. In the geometric model adopted for numerical computations the following were selected:

- three adjacent fringes (of many), distant from each other by $d = 925\ nm$, which means that the angle between the interfering beams is: $2\theta \approx 70^o$ for the wavelength of the laser radiation, $\lambda = 1064\ nm$, as illustrated in Fig. 1.
- two adjacent interference fringes, distant from each other by $d = 1850\ nm$, which means that the angle between the interfering beams is: $2\theta \approx 33{,}5^o$ for the wavelength of the laser radiation, $\lambda = 1064\ nm$.

For numerical calculations, in the first place, three "beams" (interference fringes) were adopted. Each beam had the same value of radiation intensity.

In the numerical model, it was also assumed that each of the resulting interference fringes is about 250 nm wide at half height of intensity. Furthermore, it was assumed that the intensity distribution in the interference fringe in the transverse direction is in the shape of the so called "supergaussian" curve, defined by the formula:

$$Q = Q_0 \cdot \exp\left[-F\left(\frac{t-\tau}{\tau}\right)^2\right]\exp\left[-G\left(\frac{x-x_s}{R_p}\right)^4\right] \quad (34)$$

where: Q - resultant absorbed intensity; Q_0 – initial absorbed intensity, F, G – constants, $R_p = 250\ nm$ - fringe width at half height in the transverse direction.

Such assumptions were primarily dictated by the numerical model verification, in order to check:

- how far the heat affected and target material melting zone, in the range of pulse duration, reaches,
- whether adjacent laser pulses will not cause the simultaneous process of melting and ablation of material of Al layer, in the areas adjacent to the laser beams.

This means that it is desired to obtain separated adjacent areas of target material ablation with a distinct border: for a given power density, laser wavelength and angle between laser beams. Thereby, this also means that it is not desired to obtain a periodic structure, as in Fig. 2.

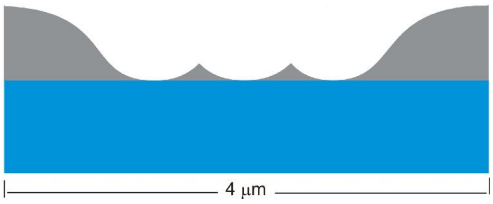

Fig. 2. Illustration of an undesired ablation effect of Al layer during illumination with a laser beam with a periodic intensity distribution

II. RESULTS AND DISCUSSION

In the first approach, in the numerical calculations, an aluminium sample irradiation (on quartz substrate) with three equidistant interference beams - fringes, generated as a result of interference of two high power laser beams, was adopted.

The equations of the problem presented in Chapter 2, for our geometric model of the sample, can only be solved by numerical methods. Taking into account the whole experience of the authors in the area of computer modelling of dynamic interactions of objects, numerical solution of equations formulated in the previous chapter by free particle method, as described in the paper [18], has been attempted.

The following values of material constants were adopted for the calculations:

– for aluminium: ρ_0= 2.78 [g/ccm], μ_0=27.6 [GPa], Q_m =397 [J/g], Q_e=1.086·10^4 [J/g], T_m = 934 [K], T_e = 2972 [K], K_0=1·10^6 [1/cm], χ_0=1.96·10^{-11} [J/(cm·s·K$^{3.5}$)], χ_1=2.37 [J/(cm·s·K)], c_{v0}=1.086 [J/(g·K)], k_1=47 [GPa], γ=2, B=0.09 [GPa], C=0.2 [GPa], E=0.0083 ,n= 0.73, m=1.7, α_1 =3 , α_2=1.4.

– for quartz: ρ_0= 2.5 [g/ccm], μ_0=28 [Gpa], Q_m =400 [J/g], Q_e =1·10^4 [J/g], T_m = 1500 [K], T_e = 3000 [K], $K0$=0 , χ_0=1.96·10^{-11} [J/(cm·s·K$^{3.5}$)], χ_1=8.8·10^{-3} [J/(cm·s·K], c_{v0}=0.63 [J/(g.K)], k_1=25 [GPa], γ=1.16, B=0.1 [GPa], C=0, E=0, m=1 , α_1 =1 , α_2 = 0.

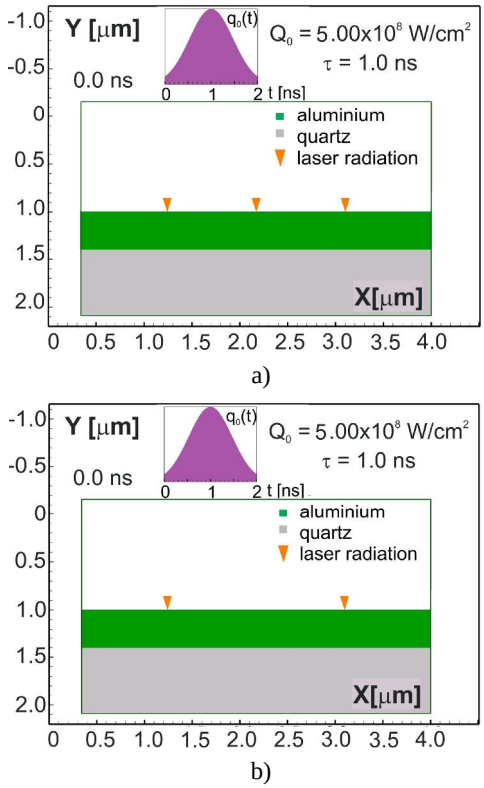

Fig. 3. Initial location of the interference fringes - "laser beams" on the target surface: a) three laser beams; b) two laser beams

The optimum duration (D) represents the duration at which minimum total cost is calculated. The disadvantage of this consideration is that, project duration might be inappropriate. It might be better to use this rule to obtain more than one solution along the crashed period as explained in Section VI.

In Figures 3a and 3b, the starting state of the samples at the beginning of their illumination with three and two

equidistant beams. In the first case, each of the beams had a power density of $5x10^8$ W/cm^2.

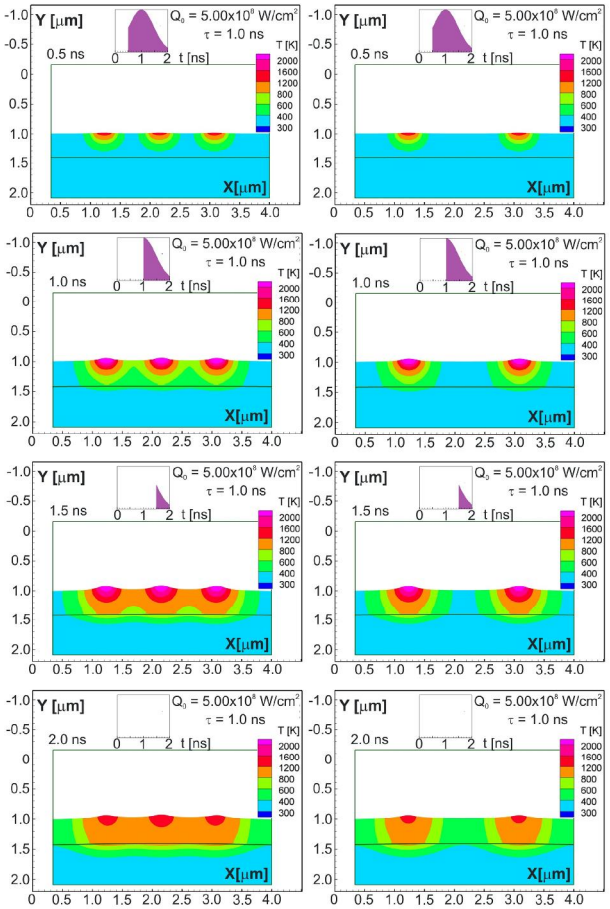

Fig. 4. Results of numerical calculations of temperature distribution in the Al layer of 400 nm during laser pulse. Power density of the laser pulse: $5 \cdot 10^8$ W/cm^2. The upper part of each figure shows the current absorbed "part" of the pulse

In Figure 4, 5 and 7, temperature distributions, calculated from the numerical model presented before, for three different power densities of laser radiation, marked on the drawings, were presented. The upper part of each figure shows a "part" of pulse duration, i.e., that part of the laser pulse, which is absorbed in the material of the target. The illustrated numerical calculations of temperature generated as a result of interaction of laser pulse with a layer of aluminium are presented in two columns in order to better compare the numerical results obtained. In the figures presented in the columns on the left side, three beams, equally spaced, every 925 nm, interact while the figures in the column on the right side, the central beam was removed. This meant that the angle between the interfering beams, in this case, was: $2\theta \approx 33{,}5^o$.

In Fig. 6 and 8, craters formed after rejection of material that was evaporated or was in the form of molten droplets of metal, respectively, for two and three beams, and power densities of the pulse $7 \cdot 10^8$ W/cm^2, were presented.

In Fig. 6a, the effect of material melting from the adjacent laser beams can be already noticed. The depth of material ablation process was stopped in the middle of the material thickness. A similar depth of the material ablation is observed in Fig. 6b, however there is a distinct separation of areas subjected to ablation.

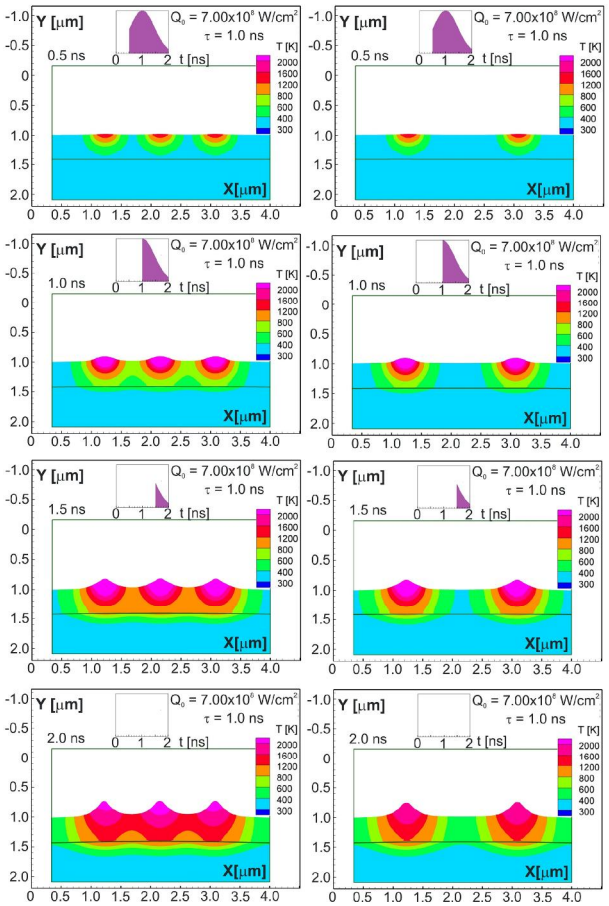

Fig. 5. Results of numerical calculations of temperature distribution in the Al layer of 400 nm during laser pulse. Power density in the laser pulse: $7 \cdot 10^8$ W/cm^2. The upper part of each figure shows the current absorbed "part" of the pulse

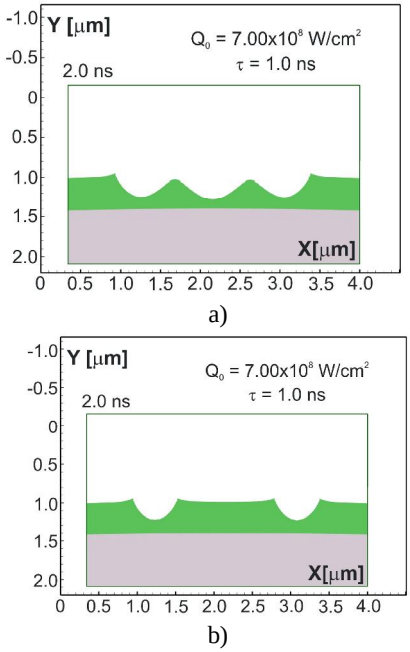

a)

b)

Fig. 6. Results of numerical calculations of the craters formed, in the Al layer of 400 nm, after the completion of laser pulse duration: a) three laser beams; b) two laser beams. Power density in the laser pulse: $7 \cdot 10^8$ W/cm^2

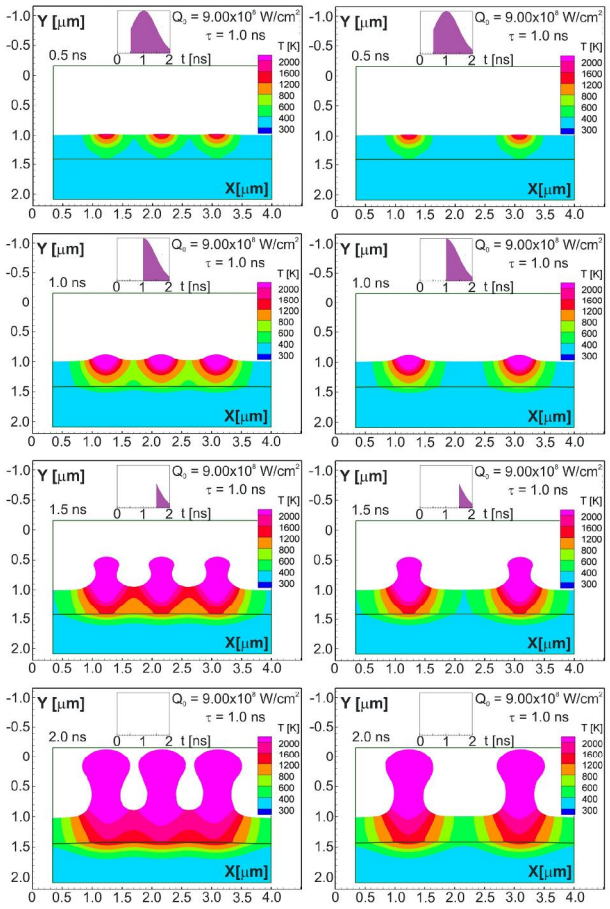

Fig. 7. Results of numerical calculations of temperature distribution in the Al layer of 400 nm during laser pulse. Power density in the laser pulse: $9 \cdot 10^8$ W/cm^2. The upper part of each figure shows the current absorbed "part" of the pulse

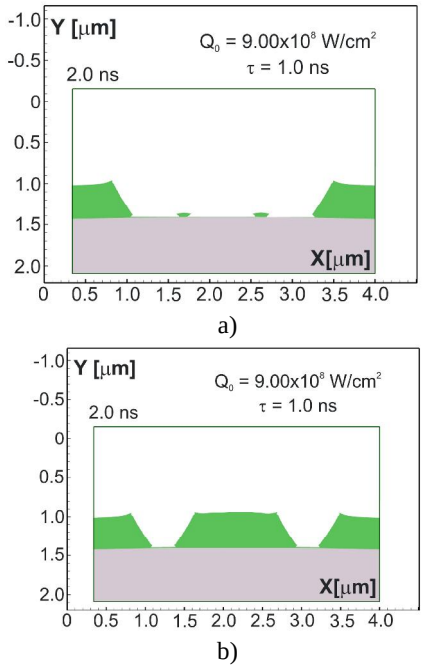

Fig. 8. Results of numerical calculations of the craters formed, in the Al layer of 400 nm, after the completion of laser pulse duration: a) three laser beams; b) two laser beams. Power density in the laser pulse: $9 \cdot 10^8$ W/cm^2

In Fig. 8a, an almost complete evaporation of A1 layer, covered by three laser beams, can be seen. In the case of two laser beams, between which the distance is doubled compared to the case of three beams, a complete evaporation of the layer deep to the substrate and a distinct boundary between the evaporated and unevaporated part of the layer, can be seen. The next step in the calculations is the maximal approach of the two beams so that the minimal distance between the interacting beams and the maximal depth of ablation could be obtained.

Conclusions of the preliminary numerical calculations for the three beams are as follows:

- For all the three simultaneously interacting laser beams, situated at a distance of 925 nm and the three adopted to calculate the intensity of laser radiation, effect of intensity (accumulation) from the individual beams can be seen and virtually the whole A1 layer evaporates (undergoes ablation).
- The distance, adopted for calculations, between the three laser beams, for all the three intensities of laser radiation is too low.
- Effect of accumulation of the temperature from the adjacent laser beams is visible - effect of heat conduction.
- The top layer of the substrate (quartz) was slightly heated for the largest intensity adopted.

In the following calculations, to quickly simplify the problem, and the time of numerical calculations, initially, the central beam involved in the interaction with the target has been abandoned. This means that the distance between interference fringes doubled. Results of numerical simulation for the interaction of two, and not three, laser beams distant from each other at 1850 nm, are shown, respectively, in Fig. 4, 5, 6, 7 and 8 on the right side. For the calculations, the same power densities of radiation were adopted.

As can be seen in Fig. 8b, as a result of numerical simulation performed for the interaction model adopted, two laser beams spaced at twice the distance compared to the first case, the following was obtained:

- Separation of ablation areas of the target material.
- Substrate temperature does not reach the melting temperature.
- Possibility to further optimise the calculations (e.g., shortening the distance between the beams) to obtain a borderline case, i.e., so that "aspect ratio", or a ratio of the depth of ablation groove of target material to the distance between "grooves" be possibly the highest.
- The modelling results have shown that the theoretical model and computer code can be successfully used for numerical simulation of the interaction of laser pulses with multilayer target consisting of different materials.

In all the figures obtained from numerical calculations, so as not to obscure the image, only temperature ranges of interest are indicated.

EXPERIMENTAL RESULTS

The experiment used a two-channel Nd:YAG laser system with resonator Q -modulation. The maximum output power

of each channel had a value of about 2 J, the laser pulse duration being of about 7 ns. Generation of the laser pulse with a duration of 1 ns is not difficult, but very expensive. Dual-channel laser system at the same time was constituted by Mach-Zehnder interferometer, the laser radiation amplifiers being arranged in its arms, which resulted in easy adjustment of light intensity in the interfering beams. The practical advantage of this system is almost automatic alignment of optical paths. Easy modification of the interference angle of the two laser beams in a fairly wide ranges was another one. In the case of depolarisation of initially polarised laser beam, as a result of thermal birefringence phenomenon in laser rods, additionally, two polarisers were installed on the output. Optical system used in the experiment for direct interference lithography is described in [26].

Although the laser pulse duration was about 7 ns, in Fig. 9, a separation of interference structure in A1 layer is clearly visible, and the obtained period of the linear structure coincides with the period of Fig. 6b and 8b.

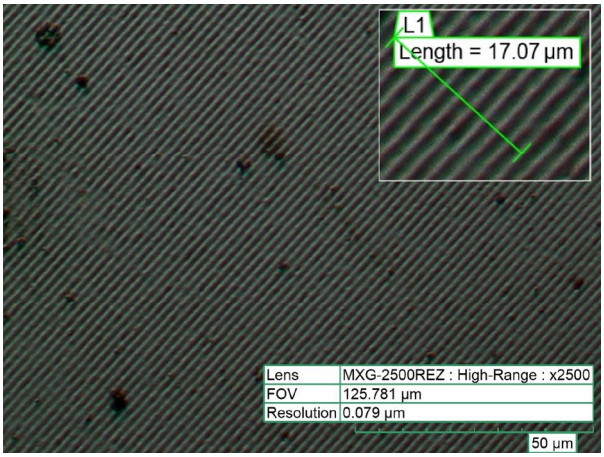

Fig. 9. Image of periodic structure from an optical microscope. Upper-right small photograph shows length of ten structure periods equal to 17.07 µm

CONCLUSIONS

The use of high power lasers in direct modification and structuring of surface layers of materials (including hardly fusible metals, sintered carbides and ceramics) is increasingly popular. Modification of the surface layers of materials leads to a variety of properties of the surface itself, providing and meeting a number of physical, chemical and mechanical requirements. This technique involves technologies, such as remelting, structuring and shock peening. In this paper, the authors present numerical and experimental results of the simultaneous interaction of multiple beams, pulsed laser radiation with a real sample model. This technology is used in the so-called direct interference lithography. The sample constituted system of a thin metallic Al layer, vapour-deposited on the quartz substrate. The objective of numerical calculations was to optimise the process of Al material ablation, which is to produce a periodic structure with the greatest depth and the minimum distance between the fringes, by means of pulsed laser radiation and a wavelength of 1064 nm. The developed numerical model is highly versatile and correctly shows the qualitative and quantitative behaviour of the irradiated object. It can be used when describing the simultaneous interaction of multiple laser beams with the sample, at any time intervals and in a fairly wide range of power densities used of laser pulses, provided in the introduction of this article.

Numerical calculations were performed for a laser pulse with a duration of 1 ns with full width at half maximum (FWHM) intensity and for such a power density of laser radiation, that the temperature of evaporation of the target material (also the melting zone of the material) of one beam does not affect the temperature of the evaporating material from an adjacent beam. It should be noted here that the numerical calculations for the adopted model geometry (aluminium on quartz) are complex, and the experimental studies even more. For such thin layers of virtually any metal, the quartz substrate constitutes a thermal buffer, which does not only make it difficult to calculate, but requires very precise experimental conditions in order to avoid the metal layer defoliation.

The purpose of these numerical calculations was to combine the method, described above, of laser interference structuring of surface for further advanced microstructure designs with the micro-plastic treatment of metal and plastic materials to form multi-level hierarchical periodic textures on surfaces including different micro-scales.

Regardless of the above-mentioned facts, the photonic method for formation of micro- and submicron structures have several advantages due to the remote and non-contact processing, flexibility during the material processing and precise dosage of energy.

According to the authors' knowledge, this is the first such approach to the numerical solution of the target material ablation process during its simultaneous illumination with many high power pulsed laser beams, adjacent to each other.

ACKNOWLEDGMENT

Presented work was partially supported by a grant 2326/B/T02/2011/40 from the National Science Centre in Poland.

REFERENCES

[1] J.H. Jang, C.K. Ullal, M. Maldovan, T. Gorishnyy, S. Kooi, C.Y. Koh, E.L. Thomas, 3D micro- and nanostructures via interference lithography, Adv. Funct. Mater. 17 (2007) 3027-3041.

[2] D. Xia, Z. Ku, S.C. Lee, S.J.R. Brueck, Nanostructures and functional materials fabricated by interferometric lithography, Adv. Mater. 23 (2011) 147-179.

[3] A. Lasagni, M.R. Nejati, R. Clasen, F. Mücklich, Periodical surface structuring of metals by laser interference metallurgy as a new fabrication method of textured solar selective absorbers, Adv. Eng. Mater. 6 (2006) 580–584.

[4] D. Bauerle, Laser processing and chemistry, Springer Verlag, Berlin, 1996.

[5] F. Mücklich, A. Lasagni, C. Daniel, Laser interference metallurgy-periodic surface patterning and formation of intermetallics, Intermetallics 13 (2005) 437–442.

[6] J.H. Moon, J. Ford, S. Yang, Fabricating three-dimensional polymeric photonic structures by multi-beam interference lithography, Polym. Adv. Technol. 17 (2006) 83-93.

[7] Y. Ono, T. Ochi, All fourteen Bravais lattices can be fabricated by triple exposure of two-beams interference fringes, Proc. SPIE 6327 (2006) 632709.

[8] S. Weiner, W. Traub, H.D. Wagner, Lamellar bone: Structure–function relations. J. Struct. Biol. 126 (1999) 241-255.

[9] J.H. Jang, D. Dendukuri, H.T. Alan, E.L. Thomas, P.S. Doyle, A route to three-dimensional structures in a microfluidic device: Stop-flow interference lithography, Angew. Chem. Int. Edit. 46 (2007) 9027-9031.

[10] J. Marczak,K. Jach, R. Świerczyński, Numerical Modeling of laser-matter interaction in the region of „low" laser parameters, Appl Phys A-Mater 100 (2010) 725-731.

[11] N. Ganesh, I.D. Block, B.T. Cunningham, Near ultraviolet-wavelength photonic crystal biosensor with enhanced surface-to-bulk sensitivity ratio, Appl. Phys. Lett. 89 (2006) 023901–023904.

[12] H. Yu, O. Balogun, B. Li, T.W. Murray, X. Zhang, Building embedded microchannels using a single layered SU-8, and determining Young's modulus using a laser acoustic technique, J. Micromech. Microeng. 14 (2004) 1576–1584.

[13] M. Campbell, D.N. Sharp, M.T. Harrison, R.G. Denning, A.J. Turberfield, Fabrication of photonic crystals for the visible spectrum by holographic lithography, Nature 404 (2000) 53-56.

[14] M. Duarte, A. Lasagni, R. Giovanelli, J. Narciso, E. Louis, F. Mücklich, Increasing lubricant lifetime by grooving periodical patterns using laser interference metallurgy, Adv. Eng. Mater. 10 (2008) 554–558.

[15] M.L. Wilkins, Computer simulation of dynamic phenomena, Springer, London and New York, 1999.

[16] D.J. Steinberg, S.G. Cochran, M.W. Guinan, A constitutive model for metals applicable at high-strain rate, J. Appl. Phys. 51 (1980) 1498.

[17] S. Kaliski, Cz. Rymarz, K. Sobczyk, E. Włodarczyk, Waves, PWN, Warsaw & Elsevier, Amsterdam, Oxford, New York, Tokyo, 1992.

[18] K. Jach, A. Morka, M. Mroczkowski, R. Panowicz, A. Sarzyński, W. Stępniewski, R. Świerczyński, J. Tyl, Computer modeling of bodies dynamic interaction using free points method, PWN Warszawa, 2001, in Polish.

[19] H. Yuan, H. Tong, M. Li, C. Sun, Computational study of nanosecond pulsed laser ablation and the application to momentum coupling, J. Appl. Phys. 112 (2012) 023105

[20] M.A. Ordal, L.L. Long, R.J. Bell, S.E. Bell, R.R. Bell, R.W.jr Alexander, C.A. Ward, Optical properties of the metals Al, Co, Cu, Au, Fe, Pb, Ni, Pd, Pt, Ag, Ti, and W in the infrared and far infrared, Appl. Optics 22 (1983) 1099-1119.

[21] V.I. Mazhukin, V.V. Nossov, I. Smurov. G. Flamant G, Modeling of radiation transfer in low temperature nanosecond laser-induced plasma of Al vapour, J. Phys. D Appl. Phys 37 (2003) 185-199.

[22] G.V. Ivanenkov, W. Stępniewski, Three-Temperature Model for the Dynamics of a Plasma Produced by Exploding Metal Wires, Plasma Phys. Rep. 26 (2000) 21-32.

[23] S. Yu. Guskov, V.B. Rozanov, M.A. Rumyantseva, Equations of state for metals (Al,Fe,Cu,Pb), Polyethylene, carbon, and boron nitride as applied to problems of dynamical compression, J. Russ. Laser Res. 18 (1997) 311-342.

[24] L.A. Merzhievskii, M.S. Voronin, Modeling of Shock-Wave Deformation of Polymethyl Metacrylate, Combust. Explo. Shock+ 48 (2012) 226-235.

[25] D.J. Steinberg, C.M. Lund, A constitutive model for strain rates from 10^4 to 10^6 s^{-1}, J. Appl. Phys. 65 (1989)1528.

[26] J. Marczak, A. Rycyk, A. Sarzyński, M. Strzelec, J. Kusiński, R. Major, Direct laser manufacturing of 1D and 2D micro- and submicro-scale periodic structures, Proc. SPIE 8703 (2013) 87030F.